PNAS RESEARCH ARTICLE | APPLIED BIOLOGICAL SCIENCES

Discovery of an LSD1 PROTAC degrader

Amir Hosseini[a,1], Xing Qiu[b,c,d,1], Yan Xiong[b,c,d,2], Ki Him Nicholas Chiang[a], Jerrel Catlett[b,c,d], Ines Kaltheuner[a], Zhijie Deng[b,c,d], Sudipta Ghosh[a], Yang Shi[a,2], and Jian Jin[b,c,d,2]

Affiliations are included on p. 8.

Contributed by Yang Shi; received December 12, 2024; accepted April 11, 2025; reviewed by Ali Shilatifard and Liling Wan

Aberrant expression of lysine-specific demethylase 1 (LSD1) has been implicated in various cancers, including acute myeloid leukemia (AML). Recent studies have revealed both catalytic and noncatalytic oncogenic functions of LSD1, which cannot be effectively addressed by traditional small-molecule inhibitors. Therefore, to remove LSD1 and mitigate its oncogenic activity, we utilized the proteolysis-targeting chimera (PROTAC) approach and developed an LSD1 PROTAC degrader MS9117, which recruits the E3 ligase cereblon (CRBN). MS9117 induces LSD1 degradation in a concentration-, time-, CRBN-, and proteasome-dependent manner. Importantly, MS9117 effectively degrades LSD1 and demonstrates superior antiproliferative effects in AML cells, compared to the existing pharmacological LSD1 inhibitors. Furthermore, MS9117 also sensitized non-acute promyelocytic leukemia AML cells to all-trans retinoic acid treatment. Moreover, we developed two negative controls of MS9117, MS9117N1 and MS9117N2, which do not degrade LSD1 or inhibit leukemia cell growth, further confirming the mechanism of action of MS9117. Overall, MS9117 serves as a valuable chemical tool and a potential therapeutic to target both the catalytic and scaffolding functions of LSD1. With several LSD1 inhibitors already in clinical development, the LSD1 degraders such as MS9117 offer an additional option for future clinical studies.

LSD1 | degrader | PROTAC | AML | ATRA

Significance

The scaffolding role of lysine-specific demethylase 1 (LSD1), beyond its catalytic function, is critical in acute myeloid leukemia (AML) progression. Here, we report the development of MS9117, a potent PROTAC degrader that effectively induces LSD1 degradation. Compared to current inhibitors, MS9117 more strongly suppresses AML cell proliferation and promotes differentiation. Therefore, MS9117 represents a powerful chemical tool compound to study broader roles of LSD1 in AML and a potential therapeutic, especially when combined with all-trans retinoic acid for potential clinical applications in nonacute promyelocytic leukemia AML.

Epigenetic dysregulation is a key feature of both solid and hematological cancers, offering promising avenues for therapeutic intervention (1–3). Histone demethylases, particularly lysine-specific demethylase 1 (LSD1), have emerged as actionable targets due to their roles in tumor development and progression (4–6). LSD1 is overexpressed in AML and various solid tumors (5, 7, 8). Its critical function in cancer stem cells suggests that inhibiting LSD1 could yield substantial clinical benefits. Moreover, LSD1 is essential for the development and maintenance of mixed-lineage leukemia (MLL)-rearranged leukemia, in cooperation with the oncogenic MLL-AF9 fusion protein (7). As a histone demethylase, LSD1 has been the target of several inhibitor development efforts aimed at treating cancers (5).

LSD1 functions as a flavin-containing amine oxidase, primarily acting as a transcriptional corepressor by demethylating histone H3 at lysine 4 (H3K4me1/2) (9). Early inhibitors, such as tranylcypromine (TCP), were shown to irreversibly inhibit LSD1 by covalently binding to its cofactor flavin adenine dinucleotide (FAD). Although TCP demonstrated some clinical activity especially when combined with all-trans retinoic acid (ATRA) in AML, its lack of specificity and side effect profile limited its effectiveness (10, 11). To overcome these challenges, more potent and specific LSD1 inhibitors, such as Iadademstat (ORY-1001), Bomedemstat (IMG-7289), and reversible LSD1 inhibitor CC-90011, have been developed and are currently under clinical investigations (12–14). These inhibitors aim to modulate LSD1's role in myeloid transcription factor networks involved in leukemogenesis. Recent advances have highlighted the importance of LSD1's dual role, not only as an enzyme but also as a scaffolding protein that stabilizes protein complexes crucial for AML pathology (15–17). Even when LSD1's enzymatic function is inhibited, its scaffolding role, particularly in interacting with transcription factors like GFI1, remains crucial for AML progression (15–17). Therefore, targeting both the enzymatic and scaffolding functions of LSD1 is necessary to fully block the differentiation arrest and leukemia progression.

PROTAC is a new type of heterobifunctional small molecule that promotes the degradation of the specific target protein by harnessing the cell's natural ubiquitin–proteasome system (18–20). This targeted degradation approach is catalytic, potentially offering higher potency than traditional small-molecule inhibitors and enabling less frequent dosing schedules. Additionally, PROTAC could offer increased selectivity, as it must engage both the target protein and a specific E3 ligase and form a productive ternary complex to achieve

Reviewers: A.S., Northwestern University; and L.W., University of Pennsylvania.

Competing interest statement: Y.S. is a co-founder of K36 Therapeutics, Alternative Bio (ABio) Inc. and a member of the Scientific Advisory Broad of K36 Therapeutics, Alternative Bio (ABio) Inc., Epigenica AB and Epic Bio, Inc. Y.S. is also a board member of ABio Inc. and Epigenica AB. Y.S. holds equity in Active Motif, K36 Therapeutics, Epic Bio, Inc., Alternative Bio, Inc., and Epigenica AB. Y.S. serves on the Scientific Advisory Board of School of Life Sciences, Westlake University and Westlake Laboratory of Life Sciences and Biomedicine and Norway Centre for Embryology and Healthy Development. J.J. is a cofounder and equity shareholder in Cullgen, Inc., a scientific cofounder and scientific advisory board member of Onsero Therapeutics, Inc., and a consultant for Cullgen, Inc., EpiCypher, Inc., Accent Therapeutics, Inc, and Tavotek Biotherapeutics, Inc. The Jin laboratory received research funds from Celgene Corporation, Levo Therapeutics, Inc., and Cullinan Oncology, Inc. All other authors declare no competing interests.

[1]A.H. and X.Q. contributed equally to this work.

[2]To whom correspondence may be addressed. Email: yan.xiong@mssm.edu, yang.shi@ludwig.ox.ac.uk, or jian.jin@mssm.edu.

This article contains supporting information online at https://www.pnas.org/lookup/suppl/doi:10.1073/pnas.2425812122/-/DCSupplemental.

Published May 14, 2025.

effective degradation of the target protein. Furthermore, unlike the conventional small-molecule inhibitors, PROTACs can eliminate both catalytic and scaffolding functions of targeted proteins.

In this study, we report an LSD1 PROTAC degrader, MS9117, which effectively targets both catalytic and scaffolding functions of LSD1 by inducing LSD1 degradation, potentially offering a more effective therapeutic strategy against AML as a single agent or in combination with other agents such as ATRA.

Results

Design and Synthesis of CRBN-Recruiting LSD1 PROTAC Degraders. We selected CC-90011 as the LSD1 binding moiety for generating LSD1 degraders due to its high potency as a reversible small-molecule LSD1 inhibitor (IC_{50} = 0.3 nM) (14) (Fig. 1*A*) and the availability of its cocrystal structure in complex with LSD1 (PDB ID: 6W4K) (14). Analysis of the cocrystal structure revealed that the methyl group attached to the pyrimidinone ring is solvent-exposed, making it a potential exit vector (Fig. 1*A*). Therefore, we modified the methyl substitution into an acetic acid to serve as a handle to attach a linker. We designed and synthesized a series of LSD1 PROTAC degraders (compound 1 to 10) (Fig. 1*B*) by conjugating the LSD1 binding moiety with various carbon and polyethylene glycol (PEG) linkers, which were attached to Pomalidomide, a classic ligand for the E3 ligase CRBN (21–24).

Evaluation of LSD1 PROTAC Degraders in AML Cells. Since LSD1 has emerged as a promising target for AML treatment, we selected the AML cell line THP-1, which harbors the MLL-AF9 oncofusion protein, to evaluate the effectiveness of potential degraders in reducing LSD1 protein levels. As illustrated in Fig. 1*C*, compounds with carbon linkers (compounds 1 to 5) did not significantly induce LSD1 degradation. Similar results were observed for compounds with longer PEG linkers (compounds 6 and 7). Interestingly, compounds with relatively shorter PEG linkers (compounds 8 to 10) showed a more profound effect on degrading LSD1. Among them, compound 8 (PEG3) was the most potent, almost completely degrading LSD1 at both 50 and 100 nM concentrations. Inspired by this result, we did further modifications on compound 8, and designed and synthesized compounds 11 and 12. Compounds 11 and 12 have a linker length similar to that of compound 8, but the ethylene glycol moiety adjacent to the CRBN binder was replaced with an acetamide moiety (Fig. 2*A*). Compound 11 retained the nitrogen atom as the atom linking to the CRBN binder, whereas compound 12 utilized the oxygen atom instead. These two modified compounds were compared side by side with previously identified lead compound 8 by WB (Fig. 2*B*). Excitingly, compound 11 (MS9117) showed improved potency in inducing LSD1 degradation. Intriguingly, compound 12, a close analog of compound 11, showed much less activity than compound 11.

Based on the above results, compound MS9117 was selected as our lead degrader for further characterization. First, the kinetics of MS9117-induced LSD1 degradation were evaluated in THP-1 cells. As shown in Fig. 2*C*, MS9117 induced LSD1 degradation in a time-dependent manner. LSD1 degradation was observed as early as 12 h, with near-complete degradation achieved after 24 h of treatment. This effect persisted for up to 48 h, and even after 72 h, more than 80% of LSD1 remained degraded, highlighting the sustained effect of MS9117. Next, we determined that MS9117 induced LSD1 degradation in a concentration-dependent manner. Treatment with 40 nM MS9117 induced more than 50% degradation of LSD1, while 50 nM resulted in complete degradation (Fig. 2*D*). Meanwhile, "hook effect," a phenomenon observed in some PROTAC degraders (25, 26), was noted at higher concentrations (>500 nM). Since LSD1 demethylates H3K4me1, we evaluated the level of H3K4me1 in THP-1 cells treated with MS9117. The WB results clearly demonstrated that MS9117 increased the level of H3K4me1 (Fig. 2*E*). Subsequently, we assessed the effect of MS9117 on LSD1 and H3K4me1 level in other AML cell lines, including NB4 (PML-RARα), MOLM-13 (MLL-AF9), and Kasumi-1 (AML-ETO). Consistent with the

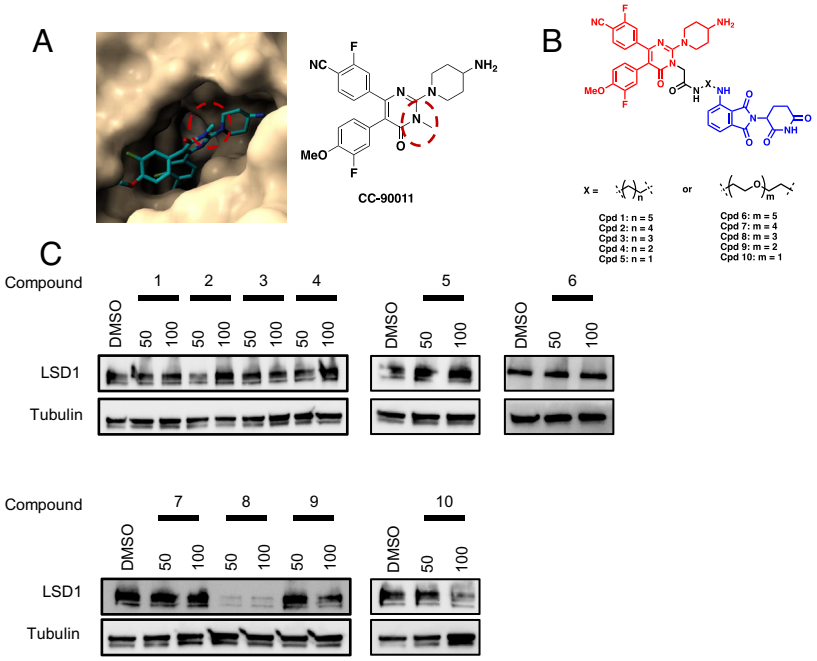

Fig. 1. Design, structures, and screening results of LSD1 degraders. (*A*) *Left*, cocrystal structure of CC-90011 in complex with LSD1 protein, PDB ID: 6W4K; *Right*, chemical structure of CC-90011. The red dashed circle indicates the solvent-exposed region of CC-90011. (*B*) Chemical structures of LSD1 PROTAC degraders **1 to 10**. (*C*) Western blot analysis of the LSD1 protein level in THP-1 cells treated with LSD1 PROTAC candidate compounds at 50 nM and 100 nM for 24 h. Tubulin was used as a loading control.

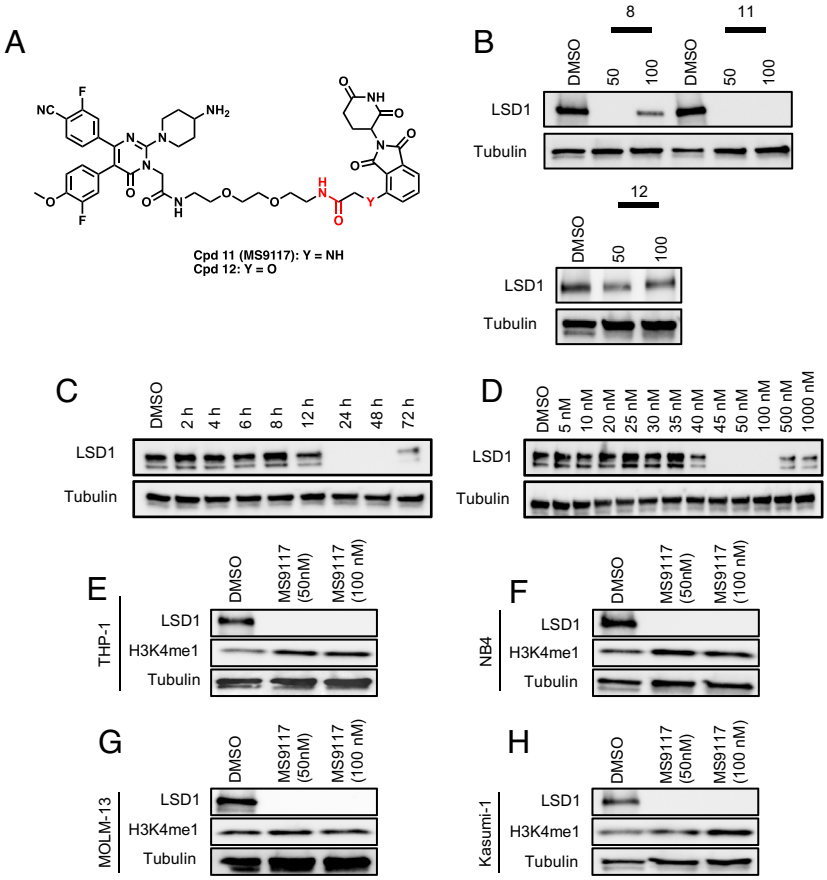

Fig. 2. Identification of the LSD1 PROTAC degrader MS9117. (*A*) Chemical structures of compounds **11** (MS9117) and **12**. (*B*) Western blot analysis of the LSD1 protein level in THP-1 cells treated with compounds 8, 11 (MS9117), and 12 at 50 nM and 100 nM concentrations for 24 h. Tubulin was used as a loading control. (*C*) Western blot analysis of the LSD1 protein level after treatment of THP-1 cells with 50 nM of MS9117 at the indicated time point. Tubulin was used as a loading control. (*D*) Western blot analysis of the LSD1 protein level in THP-1 cells after 24 h treatment with MS9117 at the indicated concentrations. Tubulin was used as a loading control. (*E–H*) Western blot analysis of LSD1 and H3K4me1 levels in (*E*) THP-1, (*F*) NB4, (*G*) MOLM-13, and (*H*) Kasumi-1 cells treated with 50 and 100 nM of MS9117 for 24 h.

observed effect on THP-1 cells, MS9117 degraded LSD1 and increased the level of H3K4me1 at both 50 and 100 nM concentrations (Fig. 1 *F–H*). Overall, compound MS9117 effectively degrades LSD1 in a time- and concentration-dependent manner and increases the level of H3K4me1.

Mechanism of Action (MOA) Studies and Selectivity Assessment for MS9117. Next, we developed two structurally similar analogs, MS9117N1 and MS9117N2, to serve as negative controls for MS9117. MS9117N1 was designed to prevent binding to the CRBN E3 ligase while still maintaining its interaction with LSD1, whereas MS9117N2 was designed to block LSD1 binding without interfering with CRBN recruitment (Fig. 3*A*). We then assessed binding of these compounds to LSD1 using Differential Scanning Fluorimetry (DSF) assays. MS9117 and MS9117N1 showed significant binding to LSD1 with thermal shifts of 12.8 ± 3.6 °C and 10.3 ± 1.7 °C, respectively, whereas MS9117N2 caused minimal temperature changes as expected (Fig. 3*B*). Next, we evaluated these two negative controls in THP-1 cells. Neither MS9117N1 nor MS9117N2 showed significant LSD1 degradation activity, indicating that LSD1 degradation mediated by MS9117 relies on its binding to both LSD1 and CRBN (Fig. 3 *C* and *D*). We also compared the cell growth inhibition effect of MS9117 with the two negative controls in THP-1 cells. MS9117 demonstrated an EC_{50} of 49 ± 10 nM, whereas MS9117N1 and MS9117N2 showed no significant inhibition of cell proliferation (<50%) at concentrations up to 4 μM after 72 h of treatment (Fig. 3*E*). These results suggest that the cell growth inhibition effect of MS9117 is likely due to its LSD1 degradation activity. Furthermore, the effect of MS9117 occurs at the posttranscriptional level, as LSD1 mRNA levels remained unaffected (Fig. 3*F*). Next, we tested the proteasomal dependency of the LSD1 degradation induced by MS9117 in THP-1 cells. As expected, LSD1 depletion by MS9117 was rescued in the presence of the proteasomal inhibitor MG-132 (27) (Fig. 3*G*), indicating that the LSD1 degradation induced by MS9117 is dependent on the proteasome. Furthermore, we performed rescue experiments in THP-1 cells pretreated with the CRBN ligand Pomalidomide (2 μM) or the LSD1 inhibitor CC-90011 (2 μM) for 24 h. Afterward, cells were treated with 50 nM of MS9117 for an additional 24 h. The LSD1 degradation induced by MS9117 was rescued by pretreatment with either Pomalidomide or CC-90011 (Fig. 3*H*). These results further supported the notion that LSD1 degradation mediated by compound MS9117 depends on binding to both LSD1 and CRBN. Since IKZF1 and GSPT1 are neosubstrates of CRBN (28, 29), we monitored their levels to ensure that the observed PROTAC activity was not due to off-target degradation of unrelated proteins. Western blot analysis confirmed that IKZF1 and GSPT1 levels remained unchanged, indicating that MS9117 selectively degrades LSD1 (Fig. 3*I*). Overall, these findings confirm that MS9117 induces LSD1 protein degradation in an LSD1-, CRBN-, and proteasome-dependent manner and is a selective LSD1 degrader.

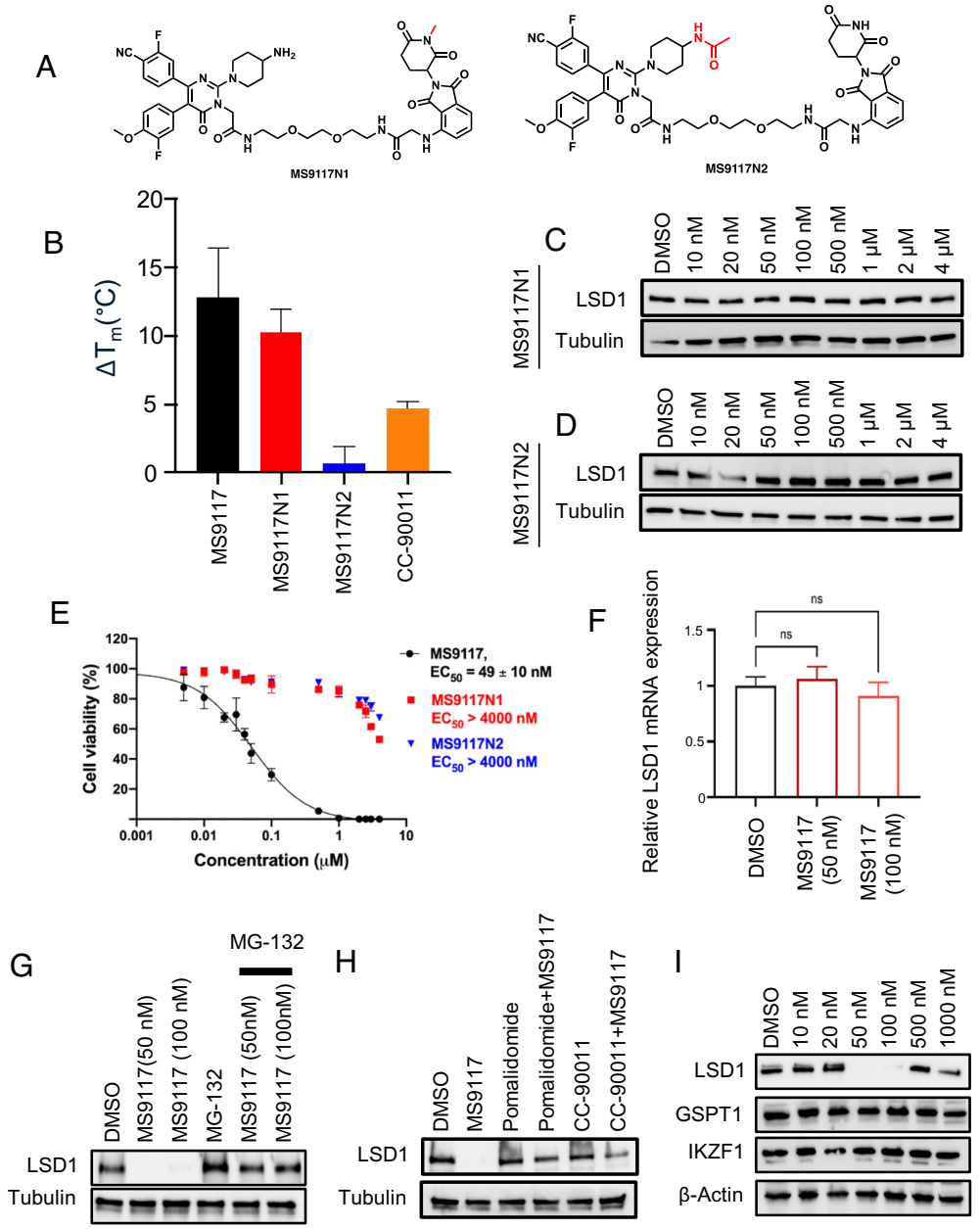

Fig. 3. MOA study of MS9117. (*A*) Chemical structures of MS9117N1 and MS9117N2. (*B*) MS9117 and MS9117N1 but not MS9117N2 induce significant thermal shifts for LSD1 at 100 μM in DSF assays (n = 3). LSD1 inhibitor CC-90011 was used as a positive control. (*C*) Western blot analysis of the LSD1 protein level in THP-1 cells after 24 h treatment with MS9117N1 at the indicated concentration. Tubulin was used as a loading control. (*D*) Western blot analysis of the LSD1 protein level in THP-1 cells after 24 h treatment with MS9117N2 at the indicated concentration. Tubulin was used as a loading control. (*E*) Cell viability of THP-1 cells treated with different concentrations of MS9117, MS9117N1, or MS9117N2 for 72 h. Luminescence signal was normalized, and dose–response curves and EC_{50} values were calculated using a nonlinear regression curve fit. (*F*) Analysis of LSD1 mRNA relative levels in THP-1 cells treated with 50 nM and 100 nM of MS9117 for 24 h. Values were normalized against *GAPDH*. *P*-values were determined using two-way ANOVA. (*G*) Western blot analysis of the LSD1 protein level in THP-1 cells after 24 h treatment with MS9117 at the indicated concentration in the presence or absence of MG-132 (2 μM). Tubulin was used as a loading control. (*H*) Western blot analysis of the LSD1 protein level in THP-1 cells pretreated with 2 μM Pomalidomide or CC-90011 for 24 h, followed by a 24 h treatment with 50 nM MS9117. Tubulin was used as a loading control. (*I*) Western blot analysis of LSD1, GSPT1, and IKZF1 protein levels in THP-1 cells after 24 h treatment with MS9117 at the indicated concentrations. β-Actin was used as a loading control.

Antileukemic Activity of MS9117. Given the role of LSD1 inhibition in suppressing AML cell proliferation and inducing differentiation, we next investigated the effect of MS9117 on proliferation and differentiation of THP-1 cells. MS9117 treatment inhibited THP-1 cell proliferation (Fig. 4*A*). Wright–Giemsa staining and light-microscopic evaluation demonstrated that compared with DMSO control, MS9117 induced a more mature morphology i.e., i) these cells contained a reduced nucleus to cytoplasm ratios and ii) increased cytoplasmic granules consistent with granulocytic or monocytic maturation (Fig. 4*B*). Cell differentiation was supported by the strongly induced expression of CD11b (Fig. 4*C*), a marker of myeloid differentiation (7, 16). We next performed a colony-forming unit assay (CFU) as a surrogate read-out for the self-renewal ability of leukemic cells. MS9117 potently inhibited the clonogenic activity of THP-1 cells (Fig. 4*D*). Treatment with MG-132 blocked the effect of MS9117 on inhibiting cell proliferation, colony formation, and inducing differentiation (Fig. 4 *A*–*D*). These results demonstrate that MS9117 effectively inhibits proliferation and promotes differentiation of THP-1 leukemic cells, and these effects are due to the proteasomal degradation of LSD1.

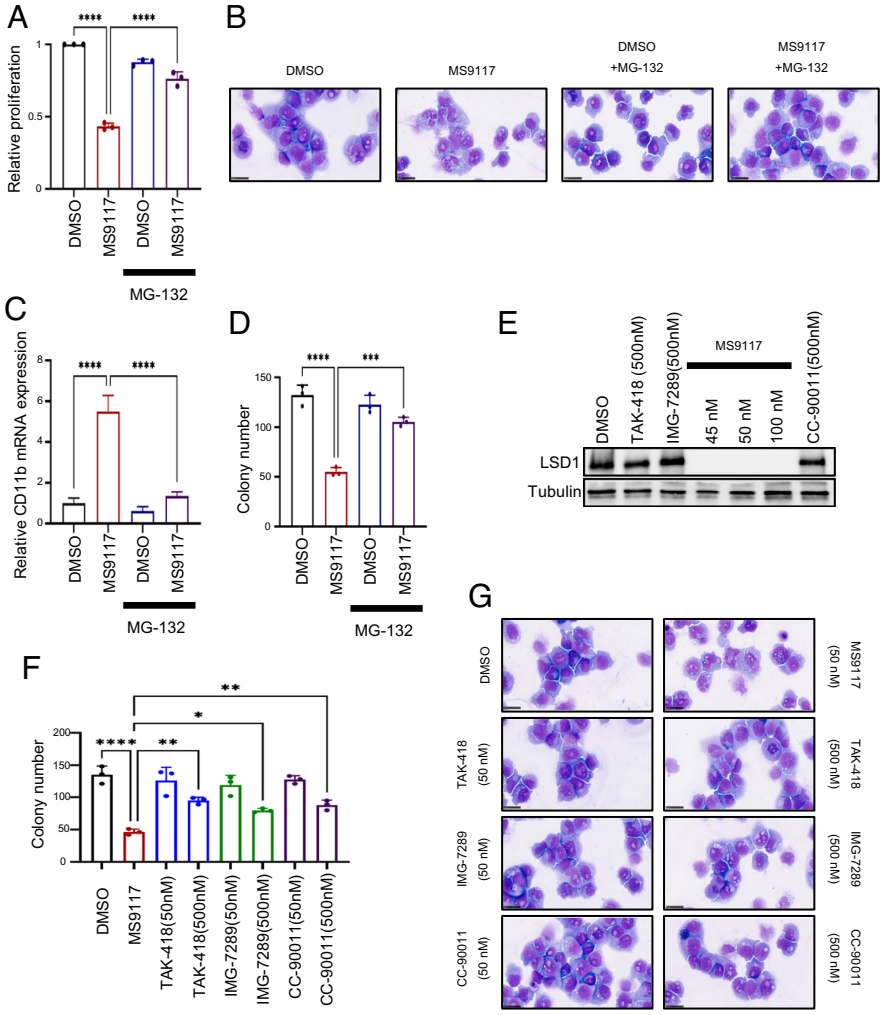

Fig. 4. MS9117 exhibits strong antileukemic activity with greater potency than LSD1 enzymatic inhibitors. (*A*) Analysis of cell viability in THP-1 cells treated with MS9117 (50 nM) for 72 h in the presence or absence of MG-132 (2 μM) by a Cell-Titer-Glo assay. *P*-values were determined using two-way ANOVA. (*B*) Representative images of THP-1 cells treated with MS9117 (50 nM) for 72 h in the presence or absence of MG132 (2 μM) and stained with Wright–Giemsa. (Scale bars, 25 μm.) (*C*) Analysis of CD11b mRNA relative levels in THP-1 cells treated with MS9117 (50 nM) for 72 h in the presence or absence of MG132 (2 μM). Values were normalized against *GAPDH*. *P*-values were determined using two-way ANOVA. (*D*) Quantification of colonies formed by THP-1 cells treated with MS9117 (50 nM) in the presence or absence of MG132 (2 μM) for 7 d Data are presented as mean of triplicates ± SD. *P*-values were determined using two-way ANOVA. (*E*) Western blot analysis of the LSD1 protein level in THP-1 cells treated with the indicated compounds at the indicated concentrations for 24 h. Tubulin was used as a loading control. (*F*) Quantification of colonies formed by THP-1 cells treated with the indicated compounds at the indicated concentrations for 7 d. 50 nM of MS9117 was used. Data are presented as mean of triplicates ± SD. *P*-values were determined using two-way ANOVA. (*G*) Representative images of THP-1 cells treated with the indicated compounds at the indicated concentrations for 72 h and stained with Wright–Giemsa. (Scale bars, 25 μm.)

Next, we compared the effect of MS9117 with several LSD1 inhibitors such as IMG-7289, CC-90011, and TAK-418. In particular, we included CC-90011 because it was utilized as the LSD1 binder in MS9117. CC-90011 is an oral, potent, selective, and reversible inhibitor, which demonstrated notable antitumor effects and an acceptable safety profile in clinical trials (14). IMG-7289 is an irreversible LSD1 inhibitor, which is currently in clinical trial for a range of hematological malignancies (13). And TAK-418 inhibits enzymatic activity of LSD1 without effect on its interaction with GFI1 (30). First, LSD1 levels were assessed by Western blot following treatment with MS9117 or LSD1 inhibitors. As expected, only MS9117 potently induced LSD1 degradation while all three LSD1 inhibitors had no effect on the protein levels of LSD1 (Fig. 4*E*). We further evaluated the effect of these compounds on clonogenic activity of THP-1 cells. THP-1 cells were treated with 50 nM MS9117, while for LSD1 inhibitors two concentrations (50 and 500 nM) were tested. MS9117 significantly inhibited the clonogenic activity of THP-1 cells at 50 nM, whereas LSD1 inhibitors had minimal effect at this concentration (Fig. 4*F*). Even at 500 nM, these LSD1 inhibitors did not achieve the anticlonogenic activity of MS9117 (Fig. 4*F*). Consistently, MS9117 induced a more mature morphology in THP-1 cells compared to these LSD1 inhibitors and significantly increased CD11b positive cells (Fig. 4*G* and *SI Appendix*, Fig. S1*A*). We then compared the effects of MS9117 with small-molecule LSD1 catalytic inhibitors on the expression of the previously reported LSD1 direct target genes *GFI1B* and *CD86* (16, 31). Consistent with LSD1 degradation over time (Fig. 2*C*), MS9117 significantly upregulated *GFI1B* and *CD86* expression, whereas LSD1 inhibitors had only a mild effect (*SI Appendix*, Fig. S1 *B* and *C*). These findings suggest that MS9117 induces a stronger and more rapid response compared to LSD1 catalytic inhibitors. Taken together, these results demonstrate that the LSD1 degrader MS9117 exhibits stronger antileukemic activity compared to LSD1 enzymatic inhibitors.

Antileukemic Activity of MS9117 in Combination with ATRA. ATRA has proven effective for the treatment of APL patients (32, 33), where combined treatment with arsenic trioxide (ATO) is curative in 95% of cases (34–37). Achieving similar effectiveness

of ATRA/ATO treatment in non-APL AML has been a major goal. And in this context, previous studies have shown that LSD1 inhibition sensitizes non-APL AML cells to ATRA treatment (38, 39), with recent findings emphasizing the crucial role of LSD1's scaffolding function in this combination therapy (16). With the LSD1 degrader MS9117 in hand, we aimed to evaluate the combination of MS9117 with ATRA in various AML cell lines.

We first used NB4 cells, an APL cell line resistant to LSD1 inhibition yet highly sensitive to ATRA, and a non-APL AML cell line, THP-1, which is sensitive to LSD1 inhibitors and resistant to ATRA treatment (16). Cells were treated with 50 nM of MS9117, with and without various concentrations of ATRA. Interestingly, MS9117 sensitized both cell lines to lower concentrations of ATRA (Fig. 5*A*). This combination treatment also strongly inhibited the clonogenic activity of THP-1 and NB4 cells (Fig. 5 *B* and *C*). In these experiments, we used two different concentrations of ATRA: a pharmacological dose (1 μM) and a low dose (10 nM). MS9117 synergistically inhibited the clonogenic activity of NB4 and THP-1 cells when combined with ATRA. Notably, the combination of MS9117 and low-dose ATRA (10 nM) had a stronger effect than TAK-418, IMG-7289, and CC-90011 combined with pharmacological dose of ATRA (1 μM) (Fig. 5 *B* and *C*).

It has been shown that differentiation therapy with ATRA leads to temporary remission (33), and the effect of ATRA is reversible, as evidenced by an increase in the number of colonies in serial

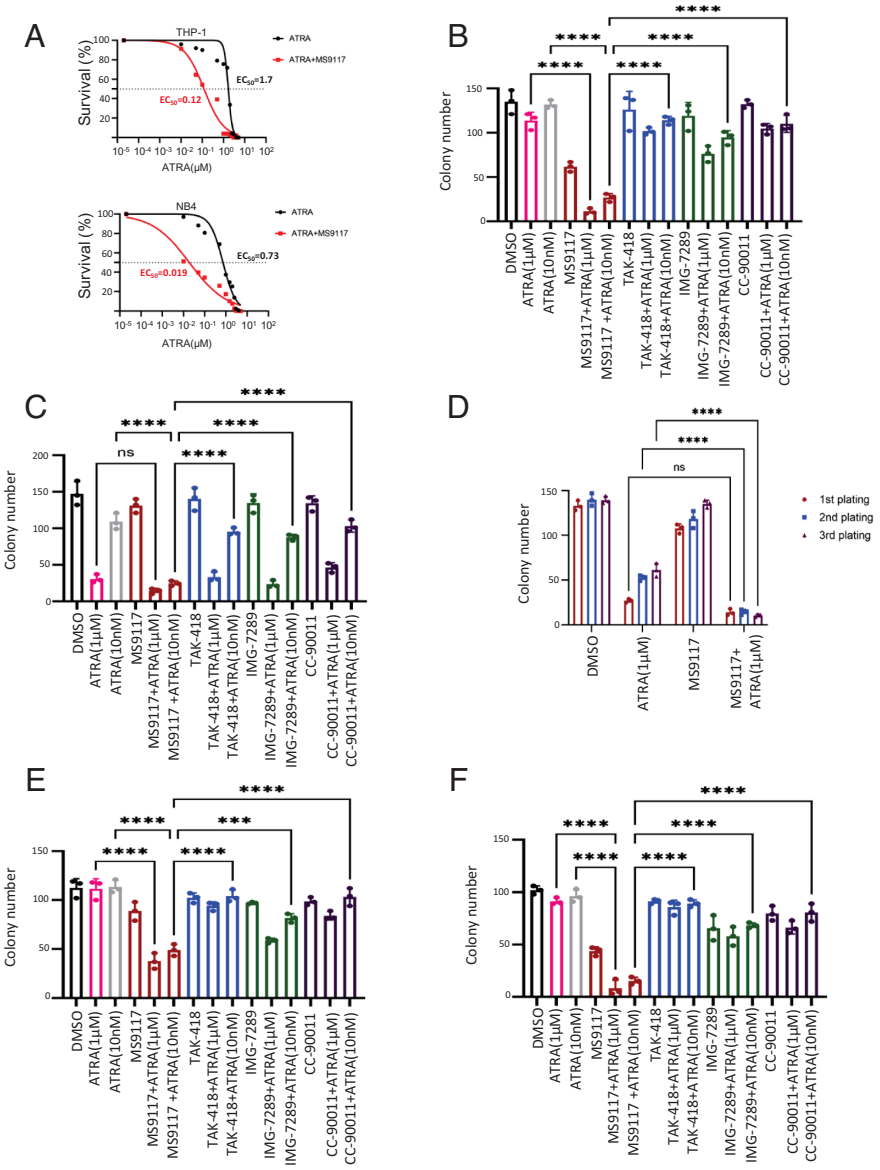

Fig. 5. MS9117 synergizes with ATRA for enhanced antileukemic activity with greater potency than other small-molecule LSD1 inhibitors. (*A*) Survival of THP-1 and NB4 cells treated with different concentrations of ATRA (black) and combination of ATRA with 50 nM MS9117 (red) for 72 h. Luminescence signal was normalized, and dose–response curves and EC_{50} values were calculated using a nonlinear regression curve fit. (*B*) Quantification of colonies formed by THP-1 cells treated with the indicated compounds at the indicated concentrations for 7 d. 50 nM of MS9117, TAK-418, IMG-7289, and CC-90011 was used. Data are presented as mean of triplicates ± SD. *P*-values were determined using two-way ANOVA. (*C*) Quantification of colonies formed by NB4 cells treated with the indicated compounds at the indicated concentrations for 7 d. 50 nM of MS9117, TAK-418, IMG-7289, and CC-90011 was used. Data are presented as mean of triplicates ± SD. *P*-values were determined using two-way ANOVA. (*D*) Analysis of the clonogenic activity of NB4 cells by serial replating assays. 50 nM of MS9117 was used. Data are presented as mean of triplicates ± SD. *P*-values were determined using two-way ANOVA. (*E*) Quantification of colonies formed by MOLM-13 cells treated with the indicated compounds at the indicated concentrations for 7 d. 50 nM of MS9117, TAK-418, IMG-7289, and CC-90011 was used. Data are presented as mean of triplicates ± SD. *P*-values were determined using two-way ANOVA. (*F*) Quantification of colonies formed by Kasumi-1 cells treated with the indicated compounds at the indicated concentrations for 7 d. 50 nM of MS9117, TAK-418, IMG-7289, and CC-90011 was used. Data are presented as mean of triplicates ± SD. *P*-values were determined using two-way ANOVA.

colony-forming assays upon ATRA withdrawal (40). To assess whether the effects of ATRA and MS9117 are reversible, we performed serial replating assays with drug washouts in NB4 cells (Fig. 5*D*). Cells from the first plating of drug-treated colonies were harvested, washed, and replated for two additional plating without drug treatment. Interestingly, in the washout and serial replating assays, while a pharmacological dose of ATRA strongly inhibited the clonogenic activity of NB4 cells in the first colony-forming assay, the number of colonies increased again in the second and third rounds after the ATRA was washed out (Fig. 5*D*). In contrast, the combination of ATRA and MS9117 maintained low colony numbers, suggesting that this combination is not reversible and may be more effective than ATRA treatment alone (Fig. 5*D*).

Finally, we extended this combination treatment to two additional AML cell lines: Kasumi-1, which is highly sensitive to LSD1 inhibitors but resistant to ATRA, and MOLM-13, which is resistant to both LSD1 inhibitors and ATRA (41). Consistent with the colony-forming assays in THP-1 and NB4 cells, MS9117 combined with ATRA synergistically inhibited clonogenic activity and exhibited a stronger effect than enzymatic LSD1 inhibitors alone or in combination with ATRA in both cell lines (Fig. 5 *E* and *F*). Next, we evaluated the effect of combining MS9117 with ATRA on the CD11b cell surface marker using FACS analysis. Consistent with the colony-forming assay and previous reports, LSD1 degradation synergistically increased the proportion of CD11b-positive cells. This effect was particularly evident at low doses of ATRA in combination with MS9117 (*SI Appendix*, Fig. S1 *D–F*). Together, these results highlight that compared to LSD1 enzymatic inhibitors alone or combined with ATRA, the combination of an LSD1 degrader and ATRA provides superior activity.

Discussion

The interplay between enzymatic versus scaffolding function of LSD1 has been investigated in the context of AML. Notably, the scaffolding function of LSD1 is particularly important for AML (16, 17), suggesting that targeting the scaffolding functions of LSD1 is critical to induce differentiation and antileukemic effects.

We identified MS9117, a highly potent LSD1-targeting PROTAC degrader that effectively degrades LSD1 in a concentration-, time-, and proteasome-dependent manner. Through rescue studies and development of two negative controls (MS9117N1 and MS9117N2), we confirmed that the LSD1 degradation induced by MS9117 is dependent on binding to LSD1 and the E3 ligase CRBN. MS9117 demonstrates superior antiproliferative effects in multiple AML cell lines when compared to previously developed LSD1 small-molecule inhibitors. Additionally, MS9117 potently synergized with ATRA to inhibit cell proliferation and clonogenic activity of AML cells. APL treated by ATRA alone has been shown to induce differentiation and only temporary remission (33, 37), in line with other studies that differentiation therapy is reversible when induced by various inhibitors (40). Consistent with these findings, our washout experiments revealed that although pharmacological doses of ATRA inhibited clonogenic activity in the NB4 APL cell line, colony formation resumed after ATRA withdrawal. Remarkably, combining MS9117 with ATRA prevented this reversibility, suggesting that this combination therapy may be more persistent and therefore effective.

While MS9117 is a promising LSD1 degrader, further optimization is needed to develop a drug candidate for clinical studies. This could be achieved by extensive modifications and optimization of the linker region with emphasis on rigid linkers (42–44), the CRBN ligands with emphasis on recently reported glutarimide-containing CRBN ligands (42–50), ligands of other E3 ligases such as VHL and DCAF1 (18–20), and LSD1 binders. Evaluation of optimized compounds alone or in combination with ATRA in in vivo mouse models with diverse AML cell lines and PDX samples is also warranted to better assess the therapeutic potential of LSD1 degraders. Overall, MS9117, an LSD1 PROTAC degrader, is a valuable chemical tool to further study LSD1 scaffolding-related mechanisms and a promising potential therapeutic for the treatment of LSD1-dependent cancers.

Materials and Methods

Cell Lines and Growing Conditions. THP-1 and NB4 cell lines were cultured in RPMI-1640 medium supplemented with 10% fetal bovine serum (FBS), 4 mM L-glutamine, and 1% penicillin-streptomycin. MOLM-13 and Kasumi-1 cells were maintained in RPMI-1640 containing 20% FBS, 4 mM L-glutamine, and 1% penicillin-streptomycin. All cells were cultured in accordance with ATCC guidelines in a humidified incubator at 37 °C with 5% CO_2 and seeded in 6-well plates for all experiments.

Inhibitors. MG-132 (HY-13259), TAK-418 (HY-138830), IMG-7289 (HY-109169B), and CC-90011 (HY-129388B) were obtained from MedChemExpress. ATRA (02190269.5) was purchased from MP Biomedicals (UK), and pomalidomide (P0018) was purchased from Sigma-Aldrich.

Recombinant GST-Tagged LSD1 Protein Purification. For protein expression, full-length LSD1 was cloned into a pGEX4T1 plasmid with an N-terminal GST-3C-tag. Recombinant protein was expressed in *Escherichia coli* BL21 (DE3) pLys cells in TB autoinduction media supplemented with 17 mM KH_2PO_4, 72 mM K_2HPO_4, 1.5% lactose, 0.05% glucose, and 2 mM $MgSO_4$ at 20 °C overnight. Cells were harvested by centrifugation and resuspended in lysis buffer (50 mM HEPES pH 7.5, 300 mM NaCl, 5 mM beta-mercaptoethanol, 0.1% NP-40, and 10% glycerol), followed by sonication. The lysate was cleared in a Beckman Avanti J-26S XP centrifuge with a JA-25.50 rotor (20,000 rpm for 30 min at 4 °C) and incubated with Pierce Glutathione Agarose (Thermo Fisher Scientific) for 30 min at 4 °C. After washing with 10 column volumes of wash buffer (50 mM HEPES pH 7.5, 1 M NaCl, and 5 mM beta-mercaptoethanol), protein was eluted in elution buffer (50 mM HEPES pH 7.5, 150 mM NaCl, 5 mM beta-mercaptoethanol, 10% glycerol, and 20 mM glutathione). Protein samples were diluted 1:10 with Heparin loading buffer (20 mM HEPES pH7.0, 100 mM NaCl, and 5 mM beta-mercaptoethanol) and loaded onto a HiPrep Heparin FF affinity column (Cytiva), followed by gradient elution to 100% Heparin elution buffer (20 mM HEPES pH7.0, 1.5 M NaCl, and 5 mM beta-mercaptoethanol). Fractions of the main peak were concentrated using Amicon Ultracentrifugal Filters (Millipore) and applied to size exclusion chromatography using a Superdex 200 PrepGrade column (Cytiva) equilibrated with SEC buffer (20 mM HEPES pH7.5, 200 mM NaCl, and 1 mM TCEP). Fractions of the main peak were pooled, concentrated, and snap-frozen in liquid nitrogen for storage at −80 °C.

Differential Scanning Fluorimetry Assay. The DSF assay protocol was performed in buffer consisting of 25 mM HEPES, 200 mM NaCl, and 1 mM TCEP used for each experiment and conducted using technical triplicates in a 96-well plate (Applied Biosystems™ MicroAmp™ Fast Optical 96-Well Reaction Plate, 0.1 mL) into an Applied Biosystems™ StepOnePlus™ Real-Time PCR System, Thermo Fisher Scientific (Catalog No. 43-766-00).

Recombinant GST-tagged LSD1 that underwent affinity and size-exclusion purification in DSF assay buffer was aliquoted at a concentration of 2.5 μM (20 μL per well) and incubated with the designated concentration of PROTAC, negative control, or inhibitor solution (20 μL per well). Finally, 10 μL of Spyro™ Orange diluted to "5×" (in DSF buffer from a stock concentration of "5,000×") was added to each well to achieve a final reaction volume of 50 μL, a final protein concentration of 1 μM, and a final Protein:Drug:Dye volume ratio of 2:2:1.

Heating was conducted using gradients from 60 to 95 °C, reading fluorescence every 0.3 °C. Raw fluorescence was plotted versus temperature and the T_m values were determined from the DSF curve inflection point, where plots of the second derivative of the raw fluorescence data for each replicate were generated and the inflection point ($d^2F/dT^2 = 0$) was estimated using the two data points between which the second derivative changes sign. The reported T_m is the average of the triplicate replicates and the reported error values are representative of the SD between the three replicates.

In Vitro Studies and Viability Assays. Cell viability was assessed using the CellTiter-Glo™ Luminescent Cell Viability Assay (Promega). Results were expressed as relative proliferation by comparing treated groups to DMSO-treated controls.

CFU Assay. Approximately 5,000 cells were plated in triplicate in methylcellulose medium (MethoCult™ GF H4435 Enriched; StemCell Technologies) presupplemented with the indicated inhibitors. For serial replating, cells harvested from colonies in the previous round were washed and reseeded in fresh methylcellulose medium. CFUs were quantified every 7 d postseeding.

Morphological Characterization (Wright–Giemsa Staining). Cells collected from culture plates were cytocentrifuged onto slides using a Cytospin™ centrifuge. Slides were then stained using the May-Grünwald-Giemsa method. Fixed cells were stained with May-Grünwald stain (Sigma-Aldrich) for 8 min, followed by six washes with deionized water. Slides were then incubated with Giemsa stain, diluted 1:19 in distilled water, for 40 min. After staining, slides were rinsed three times with distilled water and air-dried. For long-term storage, coverslips were mounted using Eukitt® mounting medium, suitable for both manual and automated applications.

Western Blot Analysis. Cells were lysed in lysis buffer containing 0.1% SDS, 400 mM NaCl, 1 mM EDTA, 50 mM Tris-HCl, and 1% Triton X-100, supplemented with protease inhibitor cocktail (Sigma-Aldrich, 11836170001). Protein concentrations were determined using the BCA Protein Assay (Promega). A total of 20 to 40 μg of protein was mixed with Laemmli buffer (Bio-Rad) and denatured at 95 °C for 10 min. Samples were then loaded onto 4 to 20% Mini-PROTEAN TGX Gels (Bio-Rad) and separated by SDS-PAGE, followed by transfer to Trans-Blot Turbo Midi Nitrocellulose membranes (Bio-Rad). Membranes were blocked in 5% BSA and incubated overnight at 4 °C with primary antibodies. The following day, membranes were washed three times with 1% TBS-T (10 min each), then incubated with the appropriate HRP-conjugated secondary antibodies diluted in 5% BSA for 30 to 60 min at room temperature. After three additional washes with 1% TBS-T, chemiluminescent substrate (ECL) was applied for signal detection. Primary antibodies used: LSD1 (ab17721), IKZF1 (sc-398265), GSPT1 (ab234433), H3K4me1 (5326S), β-Actin (4970S), Vinculin (700062), and Tubulin (sc-32293).

Surface Staining and Flow Cytometry. Cell lines were treated with inhibitors and subsequently harvested for surface staining. To block Fc receptors, cells were incubated with human TruStain FcX™ PLUS (BioLegend, Cat: 422302) for 10 min at 4 °C, followed by washing. Cells were then stained with APC-conjugated anti-human CD11b antibody (BioLegend, Cat: 101212) for 20 min at 4 °C. After washing, cells were incubated with BD FVS 575 V viability dye (BD Biosciences) for 10 to 15 min at room temperature. Following a final wash, cells were acquired using an LSRFortessa X-20 flow cytometer (BD Biosciences). Data were analyzed with FlowJo software (version 10).

Total RNA Extraction and RT-PCR. Total RNA was isolated and treated with DNaseI using the Direct-zol™ RNA MiniPrep Kit (Zymo Research, R2053) following the manufacturer's protocol. Reverse transcription of 1 μg RNA per sample was performed using SuperScript IV VILO (Thermo Fisher Scientific, 11756050) according to the manufacturer's instructions. RNA concentration was measured using a spectrophotometer (ND1000 NanoDrop). qPCR was performed with 5 to 10 ng of cDNA using SYBR™ Select Master Mix (Thermo Fisher Scientific, 4472908). All qPCR amplifications were carried out on the Step One Plus system (Applied Biosystems). Gene expression was quantified using the ΔCq method, with GAPDH as the housekeeping gene, and target expression was normalized to the global mean of the control group. Normalized fold changes were plotted using GraphPad Prism software. Primer sequences used in this study were as follows: GAPDH forward: GCCTCAAGATCATCAGCAATGC, GAPDH reverse: CCACGATACCAAAGTTGTCATGG. ITGAM (CD11b) forward: GGAGGAGAAGTGACATGGCT, ITGAM (CD11b) reverse: AGGCAAAGTGGAGATGGTGA. LSD1 forward: AGACGACAGTTCTGGAGGGTA, LSD1 reverse: TCTTGAGAAGTCATCCGGTCA. CD86 forward: CAAGACGCGGCTTTTATCTT, CD86 reverse: ATCCAAGGAATGTGGTCTGG. GFI1b forward: CAGGGAGGGGAACAGAAGAG, GFI1b reverse: GAACTGCAAAGCCTCTCTCG.

Software and Statistical Analysis. WB results shown in the figures are representative of at least two biological repeats. Statistical analyses were performed using GraphPad prism (v10.3.0) using two-way ANOVA, and statistical significance was determined at a P value < 0.05. Unless otherwise mentioned, asterisks indicate significance at these levels: $*P \leq 0.05$, $**P \leq 0.01$, $***P \leq 0.001$, and $****P \leq 0.0001$.

Data, Materials, and Software Availability. All study data are included in the article and/or *SI Appendix*.

ACKNOWLEDGMENTS. This work was supported by Ludwig Institute for Cancer Research core funding (Y.S.) and an endowed professorship by the Icahn School of Medicine at Mount Sinai (J.J.). This work utilized the NMR Spectrometer Systems at Mount Sinai acquired with funding from the NIH's SIG Grants 1S10OD025132 and 1S10OD028504 (J.J.).

Author affiliations: [a]Ludwig Institute for Cancer Research, Nuffield Department of Medicine, University of Oxford, Oxford OX3 7DQ, United Kingdom; [b]Mount Sinai Center for Therapeutics Discovery, Icahn School of Medicine at Mount Sinai, New York, NY 10029; [c]Departments of Pharmacological Sciences, Oncological Sciences and Neuroscience, Icahn School of Medicine at Mount Sinai, New York, NY 10029; and [d]Tisch Cancer Institute, Icahn School of Medicine at Mount Sinai, New York, NY 10029

Author contributions: A.H., X.Q., Y.X., Y.S., and J.J. designed research; A.H., X.Q., K.H.N.C., J.C., I.K., Z.D., and S.G. performed research; A.H., X.Q., Y.X., K.H.N.C., J.C., I.K., Z.D., S.G., Y.S., and J.J. analyzed data; Y.S. and J.J. supervision and funding acquisition; and A.H., X.Q., Y.X., Y.S., and J.J. wrote the paper.

1. M. Esteller *et al.*, The epigenetic hallmarks of cancer. *Cancer Discov.* **14**, 1783–1809 (2024).
2. M. Berdasco, M. Esteller, Aberrant epigenetic landscape in cancer: How cellular identity goes awry. *Dev. Cell* **19**, 698–711 (2010).
3. E. M. Michalak, M. L. Burr, A. J. Bannister, M. A. Dawson, The roles of DNA, RNA and histone methylation in ageing and cancer. *Nat. Rev. Mol Cell Biol.* **20**, 573–589 (2019).
4. J. W. Højfeldt, K. Agger, K. Helin, Histone lysine demethylases as targets for anticancer therapy. *Nat. Rev. Drug Discov.* **12**, 917–930 (2013).
5. A. Hosseini, S. Minucci, A comprehensive review of lysine-specific demethylase 1 and its roles in cancer. *Epigenomics* **9**, 1123–1142 (2017).
6. H. Ü. Kaniskan, M. L. Martini, J. Jin, Inhibitors of protein methyltransferases and demethylases. *Chem. Rev.* **118**, 989–1068 (2018).
7. W. J. Harris *et al.*, The histone demethylase KDM1A sustains the oncogenic potential of MLL-AF9 leukemia stem cells. *Cancer Cell* **21**, 473–487 (2012).
8. H. M. Mohammad *et al.*, A DNA hypomethylation signature predicts antitumor activity of LSD1 inhibitors in SCLC. *Cancer Cell* **28**, 57–69 (2015).
9. Y. Shi *et al.*, Histone demethylation mediated by the nuclear amine oxidase homolog LSD1. *Cell* **119**, 941–953 (2004).
10. M. Wass *et al.*, A proof of concept phase I/II pilot trial of LSD1 inhibition by tranylcypromine combined with ATRA in refractory/relapsed AML patients not eligible for intensive therapy. *Leukemia* **35**, 701–711 (2021).
11. M. M. Tayari *et al.*, Clinical responsiveness to all-trans retinoic acid is potentiated by LSD1 inhibition and associated with a quiescent transcriptome in myeloid malignancies. *Clin. Cancer Res.* **27**, 1893–903 (2021).
12. T. Maes *et al.*, ORY-1001, a potent and selective covalent KDM1A inhibitor, for the treatment of acute leukemia. *Cancer Cell* **33**, 495–511.e12 (2018).
13. J. S. Jutzi *et al.*, LSD1 inhibition prolongs survival in mouse models of MPN by selectively targeting the disease clone. *Hemasphere* **2**, e54 (2018).
14. T. Kanouni *et al.*, Discovery of CC-90011: A potent and selective reversible inhibitor of lysine specific demethylase 1 (LSD1). *J. Med. Chem.* **63**, 14522–14529 (2020).
15. A. Maiques-Diaz *et al.*, Enhancer activation by pharmacologic displacement of LSD1 from GFI1 induces differentiation in acute myeloid leukemia. *Cell Rep.* **22**, 3641–3659 (2018).
16. R. Ravasio *et al.*, Targeting the scaffolding role of LSD1 (KDM1A) poises acute myeloid leukemia cells for retinoic acid–induced differentiation. *Sci. Adv.* **6**, eaax2746 (2020).
17. J. Barth *et al.*, LSD1 inhibition by tranylcypromine derivatives interferes with GFI1-mediated repression of PU.1 target genes and induces differentiation in AML. *Leukemia* **33**, 1411–1426 (2019).
18. B. Dale *et al.*, Advancing targeted protein degradation for cancer therapy. *Nat. Rev. Cancer* **21**, 638–654 (2021).
19. M. Békés, D. R. Langley, C. M. Crews, PROTAC targeted protein degraders: The past is prologue. *Nat. Rev. Drug Discov.* **21**, 181–200 (2022).
20. J. M. Tsai, R. P. Nowak, B. L. Ebert, B. E. S. Fischer, Targeted protein degradation: From mechanisms to clinic. *Nat. Rev. Mol. Cell Biol.* **25**, 740–757 (2024).
21. T. Ito *et al.*, Identification of a primary target of thalidomide teratogenicity. *Science* **327**, 1345–1350 (2010).
22. E. S. Fischer *et al.*, Structure of the DDB1-CRBN E3 ubiquitin ligase in complex with thalidomide. *Nature* **512**, 49–53 (2014).
23. P. P. Chamberlain *et al.*, Structure of the human Cereblon-DDB1-lenalidomide complex reveals basis for responsiveness to thalidomide analogs. *Nat. Struct. Mol. Biol.* **21**, 803–809 (2014).
24. G. E. Winter *et al.*, Drug development. Phthalimide conjugation as a strategy for in vivo target protein degradation. *Science* **348**, 1376–1381 (2015).
25. M. Pettersson, C. M. Crews, PROteolysis TArgeting Chimeras (PROTACs)–Past, present and future. *Drug Discov. Today Technol.* **31**, 15–27 (2019).
26. E. F. Douglass Jr., C. J. Miller, G. Sparer, H. Shapiro, D. A. Spiegel, A comprehensive mathematical model for three-body binding equilibria. *J. Am. Chem. Soc.* **135**, 6092–6099 (2013).

27. D. H. Lee, A. L. Goldberg, Proteasome inhibitors: Valuable new tools for cell biologists. *Trends Cell Biol.* **8**, 397–403 (1998).
28. J. Kronke *et al.*, Lenalidomide causes selective degradation of IKZF1 and IKZF3 in multiple myeloma cells. *Science* **343**, 301–305 (2014).
29. M. E. Matyskiela *et al.*, A novel cereblon modulator recruits GSPT1 to the CRL4(CRBN) ubiquitin ligase. *Nature* **535**, 252–257 (2016).
30. R. Baba *et al.*, LSD1 enzyme inhibitor TAK-418 unlocks aberrant epigenetic machinery and improves autism symptoms in neurodevelopmental disorder models. *Sci. Adv.* **7**, eaba1187 (2021).
31. J. T. Lynch, M. J. Cockerill, J. R. Hitchin, D. H. Wiseman, T. C. Somervaille, CD86 expression as a surrogate cellular biomarker for pharmacological inhibition of the histone demethylase lysine-specific demethylase 1. *Anal. Biochem.* **442**, 104–106 (2013).
32. T. X. Liu *et al.*, Gene expression networks underlying retinoic acid-induced differentiation of acute promyelocytic leukemia cells. *Blood* **96**, 1496–1504 (2000).
33. J. Ablain *et al.*, Uncoupling RARA transcriptional activation and degradation clarifies the bases for APL response to therapies. *J. Exp. Med.* **210**, 647–653 (2013).
34. X. W. Zhang *et al.*, Arsenic trioxide controls the fate of the PML-RARalpha oncoprotein by directly binding PML. *Science* **328**, 240–243 (2010).
35. J. Ablain *et al.*, Activation of a promyelocytic leukemia-tumor protein 53 axis underlies acute promyelocytic leukemia cure. *Nat. Med.* **20**, 167–174 (2014).
36. H. De Thé, P. P. Pandolfi, Z. Chen, Acute promyelocytic leukemia: A paradigm for oncoprotein-targeted cure. *Cancer Cell* **32**, 552–560 (2017).
37. H. De Thé, Differentiation therapy revisited. *Nat. Rev. Cancer* **18**, 117–127 (2018).
38. T. Schenk *et al.*, Inhibition of the LSD1 (KDM1A) demethylase reactivates the all-trans-retinoic acid differentiation pathway in acute myeloid leukemia. *Nat. Med.* **18**, 605–611 (2012).
39. C. Binda *et al.*, Biochemical, structural, and biological evaluation of tranylcypromine derivatives as inhibitors of histone demethylases LSD1 and LSD2. *J. Am. Chem. Soc.* **132**, 6827–6833 (2010).
40. M. D. McKenzie *et al.*, Interconversion between tumorigenic and differentiated states in acute myeloid leukemia. *Cell Stem Cell* **25**, 258–272.e9 (2019).
41. J. P. McGrath *et al.*, Pharmacological inhibition of the histone lysine demethylase KDM1A suppresses the growth of multiple acute myeloid leukemia subtypes. *Cancer Res.* **76**, 1975–1988 (2016).
42. S. K. Bagal *et al.*, Discovery of a series of orally bioavailable Androgen receptor degraders for the treatment of prostate cancer. *J. Med. Chem.* **67**, 11732–11750 (2024).
43. Z. Chen *et al.*, Discovery of CBPD-409 as a highly potent, selective, and orally efficacious CBP/p300 PROTAC degrader for the treatment of advanced prostate cancer. *J. Med. Chem.* **67**, 5351–5372 (2024).
44. C. Wang *et al.*, Discovery of CW-3308 as a potent, selective, and orally efficacious PROTAC degrader of BRD9. *J. Med. Chem.* **67**, 14125–14154 (2024).
45. C. E. Hendrick *et al.*, Direct-to-biology accelerates PROTAC synthesis and the evaluation of linker effects on permeability and degradation. *ACS Med. Chem. Lett.* **13**, 1182–1190 (2022).
46. J. Hu *et al.*, Preclinical evaluation of proteolytic targeting of LCK as a therapeutic approach in T cell acute lymphoblastic leukemia. *Sci. Transl. Med.* **14**, eabo5228 (2022).
47. J. A. Jarusiewicz *et al.*, Phenyl dihydrouracil: An alternative cereblon binder for PROTAC design. *ACS Med. Chem. Lett.* **14**, 141–145 (2023).
48. J. Min *et al.*, Phenyl-glutarimides: Alternative Cereblon binders for the design of PROTACs. *Angew. Chem. Int. Ed. Engl.* **60**, 26663–26670 (2021).
49. S. Norris *et al.*, Design and synthesis of novel Cereblon binders for use in targeted protein degradation. *J. Med. Chem.* **66**, 16388–16409 (2023).
50. C. Steinebach *et al.*, Leveraging ligand affinity and properties: Discovery of novel benzamide-type cereblon binders for the design of PROTACs. *J. Med. Chem.* **66**, 14513–14543 (2023).